Available online at www.sciencedirect.com
SCIENCE DIRECT
Planetary and Space Science 54 (2006) 844–854
Planetary and Space Science
www.elsevier.com/locate/pss

A deep search for Martian dust rings and inner moons using the Hubble Space Telescope

Mark R. Showalter[a,*], Douglas P. Hamilton[b], Philip D. Nicholson[c]

[a]SETI Institute, 515 North Whisman Road, Mountain View, CA 94043, USA
[b]Department of Astronomy, University of Maryland, College Park, MD 20742, USA
[c]Department of Astronomy, 418 Space Sciences Building, Cornell University, Ithaca, NY 14853, USA

Received 31 October 2005; accepted 4 May 2006
Available online 7 July 2006

Abstract

It has long been suspected that Mars might be encircled by two faint rings, one originating from each of its moons Phobos and Deimos. Meteoroid impacts into these moons should release clouds of dust that quickly spread out to become rings; similar dust rings have been associated with several small inner moons of the gas giants. On May 28, 2001 Mars' hypothetical ring plane appeared edge-on to Earth within weeks of its opposition, providing the best Earth-based opportunity to detect these rings in several decades. Using the Wide Field/Planetary Camera 2 (WFPC2) on the Hubble Space Telescope, we obtained a set of deep exposures off the east and west limbs of Mars to search for these hypothetical rings. No rings were detected. This result limits normal optical depths to $\sim 3 \times 10^{-8}$ for the Phobos ring and $\sim 10^{-7}$ for the Deimos ring. These limits fall at the low end of prior dynamical predictions and a factor of 1000 below previous observational limits. However, our limit for the Deimos ring is more tentative because of large uncertainties about this ring's expected shape, size and orientation. Our data set is also sensitive to small, previously undetected inner moons. No moons were detected down to a radius limit of 75–125 m. Longitudinal coverage of the region near and between Phobos and Deimos is 40–80% complete. We conclude by describing a promising opportunity for further Martian ring viewing in December 2007.

Keywords: Planetary rings; Mars; Dust; Satellites; Dynamics

1. Introduction

Faint, dusty rings are associated with several small moons in the Solar System, including all four inner moons of Jupiter, plus Pan at Saturn, Mab at Uranus (Showalter and Lissauer, 2006) and Galatea at Neptune. Such rings arise when ejecta from a moon's surface escapes and spreads out to encircle the planet. By analogy, it has been long suspected that Mars should be encircled by two faint rings of dust, one originating from each of its moons Phobos and Deimos. This idea was first proposed by Soter (1971) and has been investigated in great theoretical detail by numerous authors. A recent literature search identified 24 refereed publications discussing the anticipated properties of Mars' putative ring system, and the list of publications is still growing; see Krivov and Hamilton (1997) for a recent summary.

Meteoroids continually impact the surfaces of Phobos and Deimos, raising clouds of dust. Without external perturbations, each resulting ring would have an orbital semimajor axis a matching its source moon and a full vertical thickness $Z = 2\ a\ \sin(i)$, where i is the moon's orbital inclination. These numeric values are ($a = 9377$ km, $Z = 353$ km) for the Phobos ring and ($a = 23,436$ km, $Z = 1464$ km) for the Deimos ring. The orbital eccentricity e of each moon gives the ring a less abrupt outer boundary of radial width $2ae$. However this effect is rather small for

*Corresponding author. Tel.: +1 650 810 0234; fax: +1 650 962 9419.
E-mail addresses: mshowalter@seti.org (M.R. Showalter), hamilton@astro.umd.edu (D.P. Hamilton), nicholson@astrosun.tn.cornell.edu (P.D. Nicholson).

0032-0633/$ - see front matter © 2006 Elsevier Ltd. All rights reserved.
doi:10.1016/j.pss.2006.05.009

Phobos (285 km) and Deimos (10 km). Jupiter's "gossamer" rings, generated by the moons Amalthea and Thebe, illustrate these properties very precisely (Burns et al., 1999; Showalter et al., 2006).

However, the Martian rings are predicted to be further distorted by the subtle interplay between radiation pressure and Mars' oblateness. Unlike other known rings, the Martian rings are expected to be longitudinally and vertically asymmetric (Hamilton, 1996). The Deimos ring should be much thicker than the above prediction; for 40 μm particles, the predicted ring should be ~6000 km thick and tilted out of the equatorial plane toward the ecliptic by ~6.5°. The thickness and tilt are both due to solar radiation pressure, which is a small perturbation on Phobos dust but a much stronger one on dust in the orbit of more distant Deimos. The tilt and thickness of the Deimos dust varies with particle size, and can be larger for tinier grains.

Curiously, the center of the Phobos ring should be offset toward the Sun by roughly one Martian radius (1 $R_M = 3400$ km), while the Deimos ring should be offset away from the Sun by several R_M (Hamilton, 1996). This peculiar result follows from the dynamics of individual dust grains. Briefly, Mars' oblateness causes orbits at Phobos' distance to precess faster than Mars' mean motion around the Sun, while for Deimos, this precession is slower than Mars' mean motion. Solar radiation pressure, which drives orbital eccentricities, is very sensitive to the difference between the two motions; the resulting offsets are in opposite directions as described in detail by Hamilton (1996).

Estimates of each ring's optical depth τ are wildly uncertain, due primarily to our limited knowledge of impactor fluxes in the relevant millimeter to centimeter size range, and in the impact yields of appropriately sized ejecta particles. There is some additional uncertainty in the dynamics of ejecta after release from the source satellite. Overall the uncertainty is at least two orders of magnitude. Nevertheless numerous authors have made estimates of the possible normal optical depths of both the Phobos and Deimos rings for different dynamical scenarios; see Krivov and Hamilton (1997) for a summary. If interplanetary impactors dominate the injection of new material into the ring, then the Phobos and Deimos rings are predicted to have $\tau \sim 10^{-8}$ and 10^{-6}, respectively. Conversely, if re-impacting ring particles provide the dominant source of new material, then a ring is said to be self-sustaining (cf. Hamilton and Burns, 1994). In this case the Phobos ring's τ might be as high as 10^{-6} while the Deimos ring's τ would increase only slightly.

There have been relatively few attempts to detect the Martian rings directly. Duxbury and Ocampo (1988) used Viking images to obtain an upper limit $\tau < 3 \times 10^{-5}$. Two years later Dubinin et al. (1990) analyzed early data from the Phobos 2 spacecraft and noted strong solar wind disturbances in the plasma and magnetic fields near the orbit of Phobos. They suggested that the observations were compatible with a ring of dust or gas in this region. The Martian rings have also been sought twice using the Hubble Space Telescope (HST). P. James (HST Program GO-5493) targeted the rings with the Wide Field/Planetary Camera 2 (WFPC2) in August 1994, but the frames were saturated and unusable. B.A. Smith (Program GTO-7176) used HST's Near Infrared Camera and Multi-Object Spectrometer (NICMOS) in October 1997; results were negative and remain unpublished. No searches via stellar occultation have been attempted, but it should be noted that rings with τ below $\sim 10^{-3}$ have never been detected using this technique.

As first predicted by Hamilton (1996), a rare opportunity for Earth-based viewing occurred on May 28, 2001, when Earth crossed the nominal ring plane of Mars. This is the geometry where vertically thin, faint rings are brightest, because a maximal amount of material overlaps along the line of sight. Several faint rings have been discovered using this geometry, including Saturn's E Ring by Feibelman (1967) and Jupiter's main ring by Voyager 1 (Smith et al., 1979). Ironically, this is the same geometry in which denser rings become faintest, because the frontmost ring particles obscure everything behind them. However, for such faint rings, even in edge-on viewing, τ is low enough that mutual obscuration and shadowing of ring particles are negligible.

While edge-on viewing opportunities occur roughly twice per year, this particular ring plane crossing (RPX) was remarkable for its proximity to Martian opposition on June 22, 2001. Orbiting at 1.5 AU and with an eccentricity of 9%, Mars varies in its distance from Earth by a factor of seven. The improved spatial resolution during opposition provides a larger telescope target and correspondingly more photons; more importantly, it increases the angular separation of the hypothetical rings from the bright planetary disk. At this RPX, Mars was at a range of only 0.50 AU, ~10% beyond its closest passage to Earth. The 2001 opportunity was exceedingly rare; the last time a Martian RPX occurred with Mars so close to Earth was on June 29, 1954; the next time will be on July 9, 2033.

Nevertheless, even under these ideal circumstances, this is a difficult observation, because of all the challenges associated with detecting faint structure so close to something as bright as Mars at opposition. For the giant planets, similar observations are simplified by the ability to work in methane absorption bands, where each planet's brightness is severely reduced. The rocky surface of Mars has no such broad absorption bands. HST provided the best available instrument for this search. Advance estimates indicated that, using WFPC2, dust belts of optical depth $\tau \sim 10^{-8}$–10^{-6}, or 10–100 times below that of the main Jovian rings, could be detected. Our observations would be most sensitive to the Phobos ring, which is predicted to be extremely thin and hence benefits most from the edge-on viewing geometry. This paper describes the negative results of that search.

2. Images and processing

2.1. Observing plan

WFPC2 contains a 2×2 arrangement of CCDs, consisting of the Planetary Camera (PC) and three Wide Fields (WF2, WF3, and WF4). The WF channels are nearly identical, with a pixel scale of 0.1″ and a total field of view of 80″. The PC has finer spatial resolution (and a correspondingly smaller field of view) by a factor of 2.2. At Mars' range of 0.5 AU, these pixel scales correspond to 36 km (WF) and 16 km (PC); the instrument's point spread function makes the effective resolution a few times larger. With WFPC2, the best way to search for faint material next to a bright object such as Mars is to position the bright object in one of the four CCDs, substantially overexpose, and study the images of the faint material in adjacent CCDs. During the Saturn RPX in 1995, Nicholson et al. (1996) used this same technique successfully in an analogous study of the faint E Ring.

We were granted three orbits of HST, each providing 50 min of observing time, for our investigation (GO-8579). Each individual orbit employed a fixed pointing relative to Mars. As summarized in Table 1, we imaged both the east and west ansas in WF channels and the west ansa only in the PC. Although the PC field of view was too small to capture the Deimos ring, our goal was to obtain superior resolution on the thinner and probably brighter Phobos ring. Note that it was not possible to image the east ansa in the PC, because that would have entailed positioning Mars in a region of the focal plane where scattered light from outside the CCD is much greater.

The Martian ring system was oriented on the sky as shown in Fig. 1. HST places significant constraints on the orientation of the instruments' fields of view on the sky, based on the requirement that its solar panels remain fully illuminated at all times. During our observing window, $\pm 30^\circ$ of rotational freedom was available. Because diffraction spikes cross WFPC2 images at 45° angles, we oriented the edge-on rings to be as close to vertical as possible. The final pointing and orientation of the rings in each visit is shown in Fig. 2.

We used broadband filters to achieve optimal sensitivity to faint rings. Filters F555 and F675 W were chosen, roughly equivalent to standard V and R filters. The purpose of the two filters was to obtain crude color information on anything we might find. The limiting factor on our exposures was scattered light from Mars. Our particular concern was to avoid saturating Mars' diffraction spikes, which naturally carry over into the adjacent CCDs. The nature of this pattern is generally difficult to

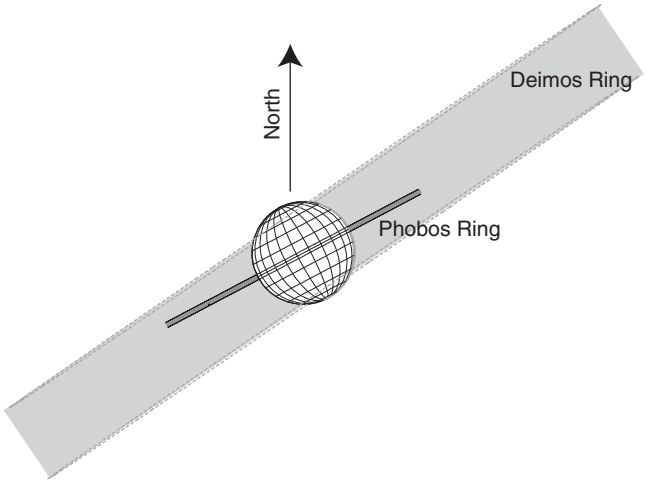

Fig. 1. This diagram illustrates the appearance of Mars and its putative ring system on 28 May 2001. Celestial north is oriented upward. Each ring is predicted to be vertically extended. The Phobos ring is shown in dark gray and the more vertically dispersed Deimos ring is shown in light gray. The rings are predicted to show asymmetries: most notably, the Deimos ring is tilted by 6.5° counterclockwise from the equatorial plane (cf. Fig. 8a of Hamilton, 1996). Both rings are also expected to be shifted radially, but that effect is primarily along a line with the Sun, so visible shifts are small when viewed so close to Mars' opposition. Nevertheless, the Phobos ring is shifted left by 700 km and the Deimos ring is shifted right by 1800 km. This diagram does not include the predicted eccentricity growth as modeled by Hamilton (1996), which arises from the interplay between planetary oblateness and solar radiation forces. This effect could extend each ring further outward by several 1000 km.

Table 1
Image summary

Visit[a]	Ring ansa	Ring CCD	Planet CCD	Image name(s)	Number of images	Filter	Exposure time (s)	Start time (UTC) on 27 May 2001
01	East	WF3	WF2	U6440101–U6440105	5	F555W	80	7:19:14
				U6440106	1	F502N	0.23	7:35:14
				U6440107–U644010E	8	F675W	50	7:38:14
02	West	WF2	WF3	U6440201–U6440205	5	F555W	80	0:53:14
				U6440206	1	F502N	0.23	1:09:14
				U6440207–U644020E	8	F675W	50	1:12:14
03	West	PC1	WF4	U6440301–U6440304	4	F555W	400	2:29:14
				U6440305	1	F555W	350	3:04:14
				U6440306	1	F502N	0.23	3:13:14

[a]Note that visit numbers are assigned at the planning stage and have no direct relationship with the ordering of the visits; in fact visit 01 executed last.

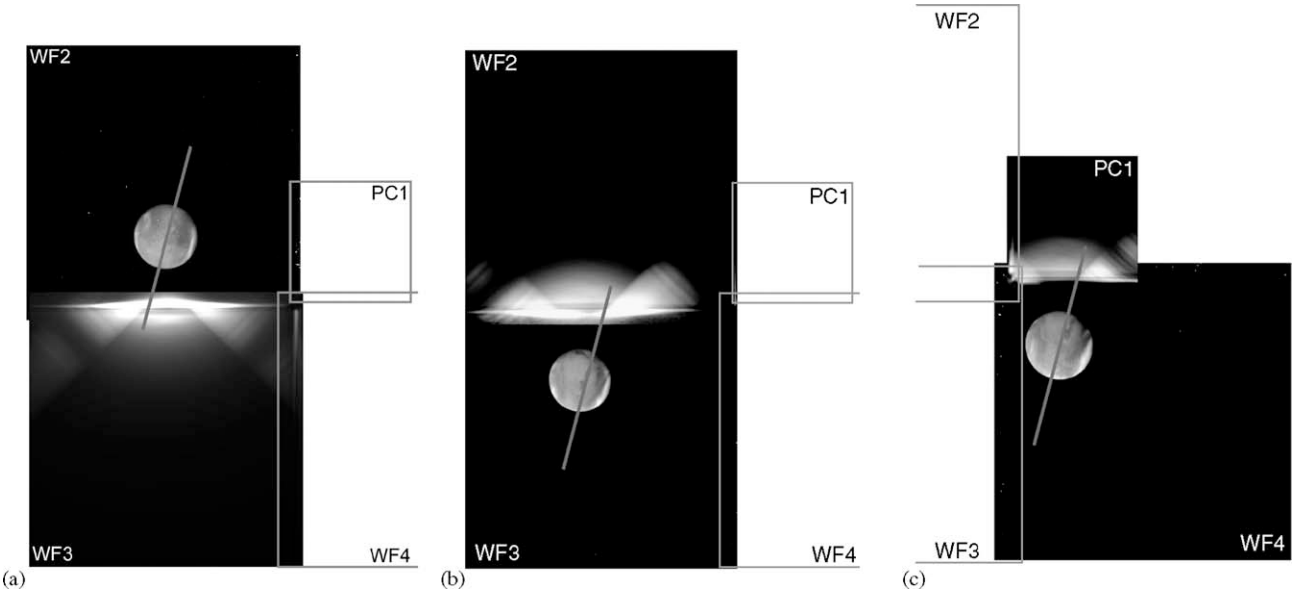

Fig. 2. These three panels show the viewing geometry for visits 01, 02 and 03, respectively. In each case, the un-saturated image of Mars is shown and a broad gray line indicates the orientation and scale of the predicted Phobos ring. The outlines of the adjacent, unused WFPC2 fields of view are also shown for context. A coadded version of each targeted frame is also shown, in which Mars' broad diffraction spikes are visible.

predict in advance. While the point spread function (PSF) of WFPC2 is reasonably well characterized, the pattern arising from Mars entails convolving the PSF across Mars' large disk. For our planning purposes, we could take advantage of an unusual coincidence—the size of Mars on the sky in May 2001 was nearly identical to the size of Saturn during the 1995 RPX, and the projected extent of the hypothetical Phobos ring was nearly identical to that of Saturn's G ring. As a result, we were able to tailor our pointings and scale our exposure times to the images obtained by Nicholson et al. (1996). With this approach, we were able to predict exposure times that were very nearly optimal (see Table 1); the brightest part of each image (along the edge closest to Mars) was close to but generally did not exceed saturation levels.

In addition, each visit included a very short exposure through the narrow-band filter F502N. This was used to provide an un-saturated image of Mars from which we could derive reliable pointing information for our images (Fig. 2). HST's tracking system is extremely reliable for Solar System targets, so a single image was deemed sufficient to characterize the pointing for an entire visit. Nicholson et al. (1996) reached similar conclusions in their prior examination of Saturn's rings.

Note that this observing plan was very specifically tailored to the properties of WFPC2. More recent HST observations of the faint rings of Jupiter, Uranus and Neptune have employed the newer Advanced Camera for Surveys (ACS) (Showalter et al., 2003, 2005a, b; Showalter and Lissauer, 2006), which has generally superior sensitivity and rejection of off-axis light. However, the ACS was not yet available in May 2001.

2.2. Image processing and calibration

Space Telescope Institute's standard, "pipeline" processing was applied to the images prior to their retrieval from the data archive. The images in this form are flat-fielded, calibrated and include a parameter called PHOTFLAM, which is defined as the mean flux density, in units of erg $\mathrm{cm}^{-2}\,\mathrm{s}^{-1}\,\text{Å}^{-1}$, that produces one image DN in 1 s (Baggett et al., 2002). Here DN refers to the "data number" values of the individual pixels in the digital image. We seek intensities I expressed via the ratio I/F, where πF is the incident solar flux density. Here intensity is defined as the incoming flux density per unit of solid angle (in steradians) on the sky. The ratio I/F has the advantages of being dimensionless, independent of the solar spectrum, and defined to equal the geometric albedo of a surface with perpendicular illumination and viewing. The quantity F can be determined from a weighted average of the solar flux density over the bandpass of the combined optics, filter and instrument. This is then adjusted for the Sun–Mars distance, 1.493 AU at the time of the observations. The final conversion factor is

$$I/F \text{ per DN} = \text{PHOTFLAM}/([T/\text{s}]\Omega F), \quad (1)$$

where T is the exposure time (in units of seconds) and Ω is the solid angle, in steradians, subtended by a pixel.

3. Ring search

3.1. The Phobos ring

Long exposures on HST tend to be littered with bright specks caused by cosmic rays hitting the CCD. Our long

exposures were particularly affected. Using a combination of median filtering and coadding, we have been able to eliminate these hits, producing relatively clean images (Fig. 3a). However, a strong gradient in scattered light remains, caused by off-axis light reflected from Mars (which would have been over-exposed by a factor of 3000 had it appeared within the field of view). We have modeled this gradient as a third-order polynomial in pixel coordinates (line, sample), which we have fitted to the small region surrounding the hypothetical ring. Upon subtraction of this polynomial (Fig. 3b), the region around the ring becomes much more uniform, with variations remaining that are about 1% as large as the original gradient. This "flattened" image would potentially show the ring if it were present. Similar processing of more recent HST images of the Jovian "gossamer" rings used the same techniques and was successful at revealing this exceedingly faint ring (Showalter et al., 2006).

We have employed a few "tricks" to push the detection sensitivity further. First, we coadd the images through the two color filters, F555 W and F675 W. Second, we attempt to coadd pixels within the image to further enhance our sensitivity. As Fig. 3c illustrates, we define a box around the vertical limits of the putative ring, and also a pair of identical boxes displaced north and south from the equator plane. We then coadd pixels as a function of projected distance from Mars' rotation axis. The final profile is generated by subtracting from the middle (ring) profile the average of the adjacent pair. This subtraction removes any residual gradient in light that may persist in the region around the ring. The resulting profile is shown in Fig. 4. Had a ring been detectable, it would have appeared as a nonzero value for I/F up to approximately 13,500 km (Hamilton, 1996), beyond which it would drop rapidly to zero. No distinctive signature of the ring can be seen. There is also no detectable change at the orbit of Phobos, where we would expect the ring boundary if the radially offset ring model of Hamilton did not apply.

At the time of observations, Earth's viewpoint off the Sun–Mars line (i.e., the phase angle α) was 14°. According to the non-axisymmetric model of Hamilton (1996; cf. Fig. 1), this should leading to an East–West asymmetry of 700 km for the Phobos ring. Thus, we might expect an offset of this magnitude in our coadded profile and, because the offset can depend on particle size, the outer edge might be somewhat less abrupt. Nevertheless, it is clear that no adjustments on scales of 700 km can alter our conclusion that no ring is detectable at a significant level.

Note that the limiting factor in this non-detection is based on systematic, not statistical uncertainties. The latter would be quite easy to derive from the standard deviation among the data points in the profile. The actual limit is based on uncertainties in the residual background variations, which are much more difficult to quantify. We must also acknowledge our uncertainties in the dust dynamics, which raise questions about how the ring really ought to look. We therefore believe it is appropriate to interpret our detection limit in Fig. 4 very conservatively, adopting $I/F < 10^{-7}$ as the upper limit on the edge-on intensity of any Phobos ring.

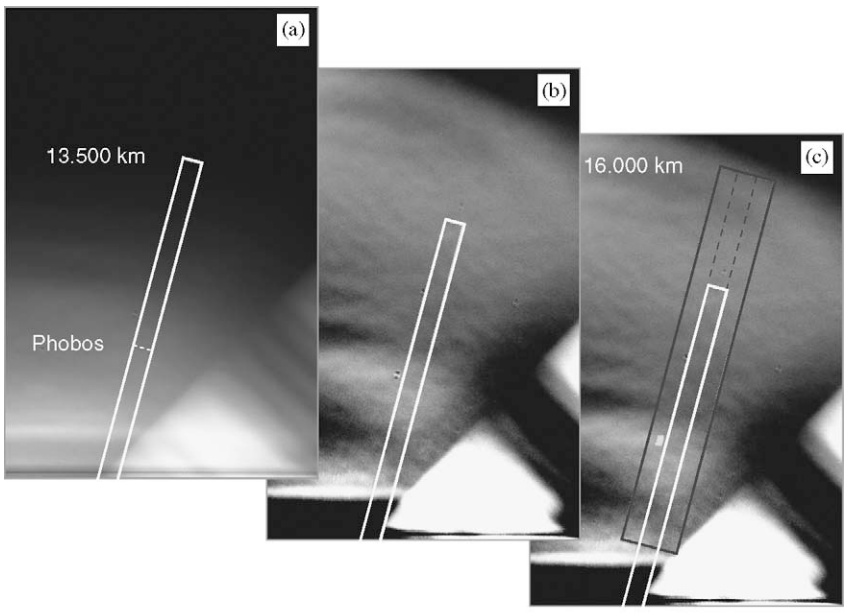

Fig. 3. Image processing steps in the search for the Phobos ring. (a) A coadded frame, composed of all the PC1 images from visit 03. The outline of the predicted Phobos ring is indicated, extending outward to 13,500 km and with a full vertical thickness of 400 km. The location of Phobos' orbit is indicated by a white dashed line. (b) The same image, after a polynomial model for the adjacent background light has been subtracted. The sensitivity of this "flattened" image is ~100 times finer than prior to the background subtraction. (c) The image after masking out corrupted pixels (light gray). The dark gray box outlines the three scan regions, consisting of a central scan atop the Phobos ring, plus additional scans above and below to model adjacent background variations. The scans extend outward to 16,000 km. The final radial scan equals the central scan minus the average of the two adjacent scans. By inspection of the image, it is already rather apparent that no Phobos ring has been detected.

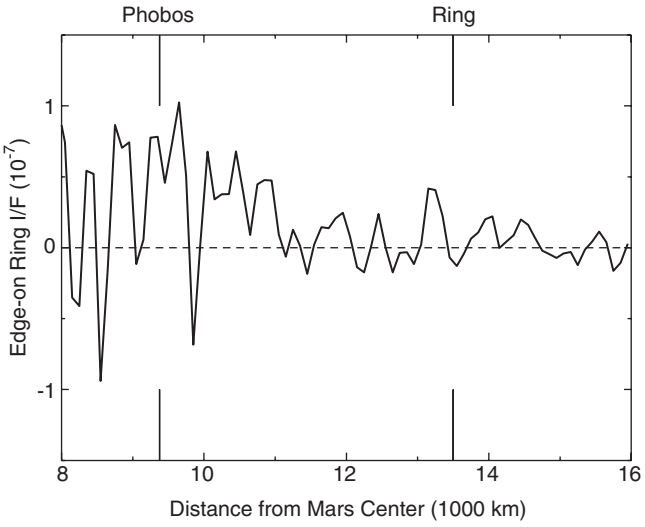

Fig. 4. A derived, edge-on profile of the Phobos ring. The radial location of Phobos' orbit is indicated, along with the predicted location of its ring's outer boundary near 13,500 km. The curve has been derived by coadding profiles from all the images from all three visits and both filters. If a detectable ring were present, one would expect to see a positive value interior to the ring limit and a zero value exterior to it. What is seen, instead, is consistent with noise. By examining the images, it is clear that the modest peak near the orbit of Phobos is related to residual background light in the images. Nevertheless, we adopt this amplitude, $\sim 10^{-7}$ in units of I/F, as a conservative upper limit on the edge-on intensity of any Phobos ring. At the ring's predicted outer boundary, the limit is ~3 times smaller.

To complete this task we must convert the ring's edge-on brightness limit to an approximate limit on the ring's normal optical depth τ. This requires several assumptions. First, we need to convert from the ring's edge-on I/F to the value that would be expected in a perpendicular view. Fig. 5 illustrates the ring geometry from both edge-on and normal viewpoints. (Variables are labeled for the Deimos ring but the same formulas apply.) The relationship indicated is

$$\text{edge-on } I/F = \text{normal } I/F \times 2\,(R^2 - X^2)^{1/2}/Z. \qquad (2)$$

For the Phobos ring, $R = 13,500$ and $Z = 353$ km. The value for X is variable within Fig. 4 but a typical value is ~9000 km. This yields a factor of ~60, so the ring's normal I/F is limited to $\sim 2 \times 10^{-9}$. In backscattered light, the normal I/F is equal to τ times the geometric albedo. Phobos and Deimos both have geometric albedos of ~0.07, so we adopt this value for the ring material as well. The final limit on the Phobos ring is $\tau < \sim 3 \times 10^{-8}$. This is comparable to the optical depths of the other faintest rings known, such as that of the Jovian gossamer rings. It is also a factor of 1000 below the detection limit established previously by Duxbury and Ocampo (1988).

3.2. The Deimos ring

Our search for the Deimos ring follows a procedure similar to that described above, except for one additional step (Fig. 6). Because the hypothetical ring is ~6000 km wide and extends almost all the way across the WF fields, scattered light from Mars becomes an even greater obstacle than in our search for the Phobos ring. However, we can take advantage of the fact that most of the scattered light is symmetric about a vertical line in WF3 and a horizontal line in WF2. Thus, we can remove much of the contamination by subtracting a mirror-reflected version of each image from itself (Fig. 6b). The predicted ring plane is tilted and offset relative to this line of symmetry so it is, for the most part, unaffected. Afterward, we again model the region around the ring by a third-order polynomial, further isolating any ring from the background variations (Fig. 6c).

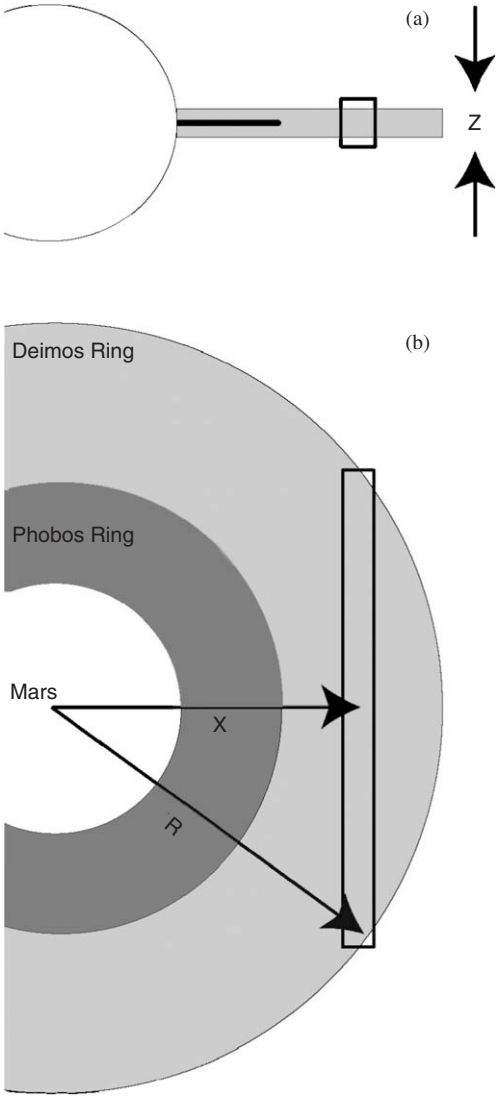

Fig. 5. A diagram of the edge-on viewing geometry and how to convert between edge-on I/F and normal I/F. (a) A side view shows a rectangular sub-region of the thick, edge-on Deimos ring. The ring thickness is defined to be Z. (b) The same view from top down shows the region of the ring that is encompassed by the edge-on measurement. The region has a mean, projected distance from the planet of X and a radius R, so the line of sight across the ring is $2\,(R^2–X^2)^{1/2}$. The conversion factor is simply the ratio of this distance to Z.

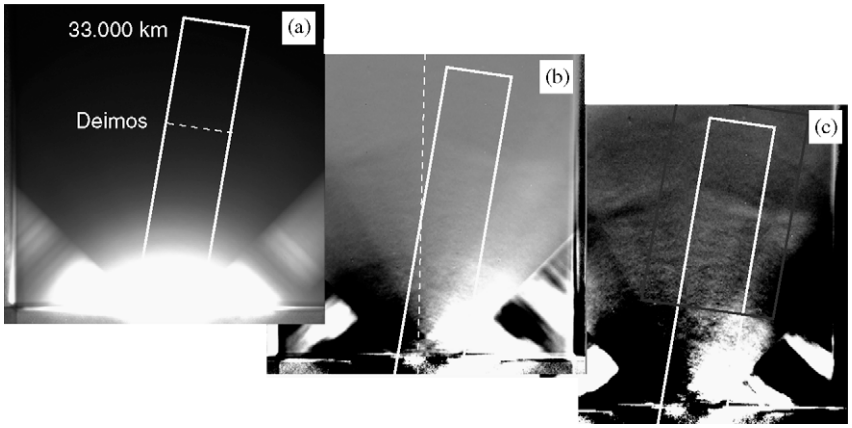

Fig. 6. Image processing steps in the search for the Deimos ring (cf. Fig. 3). (a) A coadded frame, composed of all the WF3 images from visit 01 (rotated 180° relative to Fig. 2a). The outline of the predicted ring is indicated, extending outward to 33,000 km and with a full vertical thickness of 6000 km. Based on the predictions of Hamilton (1996; cf. Fig. 1), this model ring is rotated 6.5° counterclockwise from the ring's equatorial plane. For comparison, the radial limit of Deimos' orbit is indicated by a white dashed line. (b) The same image, after a mirror-reflected duplicate has been subtracted. Because the scattered light is nearly symmetric about dashed line shown, this step removes most of the background light gradient scattered by Mars. (c) The region around the Deimos ring has been modeled by a third order, two-dimensional polynomial and subtracted. The remaining variations are ~1% as large as in the original unprocessed image. The dark gray box outlines the scan regions, consisting of a central scan atop the Deimos ring, plus additional half-width scans north and south to model any residual adjacent background variations. The final radial scan equals the central scan minus the average of the adjacent two.

As before, we combine all available data from WF2 and from WF3 in our processing. The model ring plane shown in Fig. 6 has been rotated 6.5° counterclockwise from the equatorial plane, as per the model of (1996). Finally, we generate three radial profiles as before, and subtract the mean of the outer profiles from the central (ring) profile. In this case the outer profiles are only half as wide as the central scan, because our background "flattening" procedure was grown less reliable with increasing distance from the ring plane. The result is shown in Fig. 7. Clearly residual background variations continue to dominate at the level of $I/F\sim$ a few $\times 10^{-8}$, and no ring is detectable. We have also searched for the Deimos ring assuming alternative models for its shape and orientation. For example, we can find no evidence for a ring that is equatorial. Nevertheless, it remains possible that we could have overlooked a ring comparable in amplitude to the background variations shown in Fig. 7. We therefore adopt 5×10^{-8} as an upper limit on the Deimos ring's intensity.

Eq. (2) provides the conversion factor to normal I/F. We assume $R = 33,000$, $Z\sim6000$ and $X\sim22,000$ km. The resulting factor is ~8, so normal $I/F<6 \times 10^{-9}$ and normal $\tau<\sim10^{-7}$. This limit is weaker than that for the Phobos ring because of the Deimos ring's greater vertical thickness and larger geometric uncertainties. Nevertheless, it still places the Deimos ring below a limit comparable to the optical depth of Jupiter's main ring and Saturn's G ring.

Hamilton (1996) note that a ring of tinier grains could be tilted as much as 15° and, if the ring hosts a broad range of particle sizes, it could lack the abrupt boundaries that we have assumed in the analysis above. Other more recent models (Krivov and Hamilton, 1997; Makuch et al., 2005; Krivov and Feofilov, 2006) reach similar conclusions. In short, the Deimos ring's three-dimensional structure is much more uncertain than that of the Phobos ring. Depending on the dynamical assumptions, the Deimos ring could plausibly have even exceeded the dimensions of the WF channel in 2001. If so, then the Deimos ring might have escaped our detection even at the level quoted above. Because our conclusions about this ring are dependent on the dynamical models, our conclusions should be treated as more tentative.

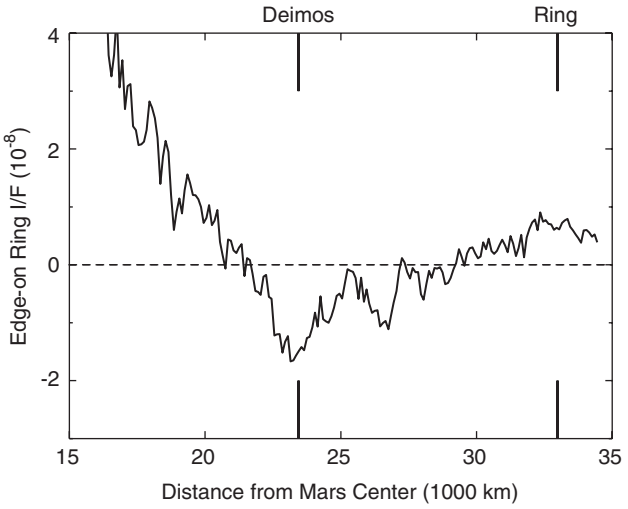

Fig. 7. A derived, edge-on profile of the Deimos ring (cf. Fig. 4). The radial location of Deimos' orbit is indicated, along with the predicted location of its ring's outer boundary (~33,000 km). The curve has been derived from all the WF3 and WF2 images of visits 01 and 02. If a detectable ring were present, one would expect to see a positive value interior to the ring's limit and a zero value exterior to it. What is seen is, instead, are residual background variations with I/F of a few times 10^{-8}.

4. Search for embedded moons

While it was not a primary goal of our observations, the images obtained were uniquely suited to detecting small, inner moons of Mars. A moon would appear as a faint streak, most likely near the equatorial plane, in our images. A moon orbiting in the range from Phobos to Deimos would have a maximum projected sky velocity relative to Mars of 0.2″/min, and considerably less if imaged near maximum elongation. Stars can be distinguished from moons by their larger sky velocities (0.5″/min) and because they move in a direction tilted from the equatorial plane by ~30°; in general very few stars were detectable in the WF channel and none in the PC (where stars smeared by ~70 pixels). Here we describe the results of a search for moons of Mars. We follow procedures similar to those of Dones et al. (2006), who searched for moons in images taken during Saturn's 1995 RPXs.

As noted above, the images show large overall gradients in brightness due to scattered light from Mars (Fig. 8a; cf. Fig. 3a). These gradients make it difficult to see a hypothetical moon clearly. Our approach to the ring search involved subtracting a polynomial background model, but that method only works for small regions of the image. To search for moons, we instead apply a high-pass filter to the data (Fig. 8b), which removes the distracting gradients and highlights tiny, isolated features. In particular, the many cosmic ray hits now appear clearly. Note that, instead of using an exact high-pass filter, we use a similar filter that has been optimized specifically for moon searches. For each pixel, the filter subtracts off the local average within a 4.5-pixel radius, but neglects any points within a 2.5-pixel radius. The inner radius has been chosen to encompass most of the instrument's PSF, so that we do not risk reducing the intensity of any actual features. Remaining features were located by eye and then tabulated and to see if any of them persisted and slowly moved from one image to the next. In this search, no believable candidate moons were located. (Automated search techniques might conceivably change this negative result, but such techniques would need to be tailored to handle the strong, non-random background variations and the numerous cosmic ray hits in these images.)

We can estimate our sensitivity to small moons by adding arrays of very tiny moons to a sample WF image (Fig. 8c). We match the PSF of the image and add moons whose brightnesses change in steps of $\sqrt{2}$. The moons were added at different lines within the image to explore how our sensitivity varies across the frame. Noise is largest closer to the planet, where scattered light is more intense, so we expect reduced sensitivity in this region. Nevertheless, we find that we are sensitive to extremely small bodies in orbit about Mars, with radii in the range 75–125 m (again assuming a geometric albedo of 0.07). The smaller limit applies at the largest radii, beyond Deimos, whereas the larger limit applies in the region closer to Phobos. For comparison, Phobos and Deimos have radii of ~10 and ~6 km, respectively.

How complete was our search? Fig. 9 shows the fractional coverage in longitude as a function of orbital radius. It is based on the assumption that moons follow orbits that are prograde, nearly circular and nearly equatorial. Coverage is generally 70–80% complete in the region around Deimos. It drops rapidly interior to Phobos where glare from the planet was too intense. The peak at the orbit of Phobos reflects the fact that our observations were timed to avoid the presence of either known moon; hence our visits were in some way commensurate with Phobos's orbital period.

The detection limits and completeness estimates are based primarily on an analysis of the WF images, where the expected smear of a moon is rather small. For the PC

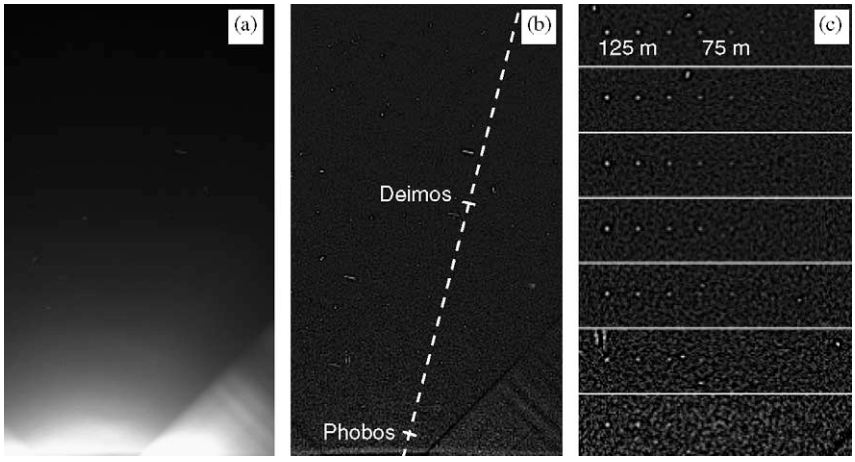

Fig. 8. Steps in the search for small, unseen moons of Mars. (a) A WF2 image of the rings from visit 02 (rotated 90° relative to Fig. 2b). Scattered light from Mars is visible along the bottom and Mars' diffraction spike is at lower right. (b) The same image after high-pass filtering, as described in the text. The edge-on equatorial plane is shown as a dashed line, and the orbital radii of Phobos and Deimos are indicated. (c) Closeup strips from the same image in which we have added a sequence of sample moons, decreasing in brightness from left to right in steps of $\sqrt{2}$. Moons of radius 125 and 75 m are labeled in the first strip. The strips are taken from regions distributed from the top to the bottom of the frame. Because of the increased scattered light at the bottom, moons are more difficult to detect in this region. Nevertheless, a 125-m moon would be visible almost anywhere in an image.

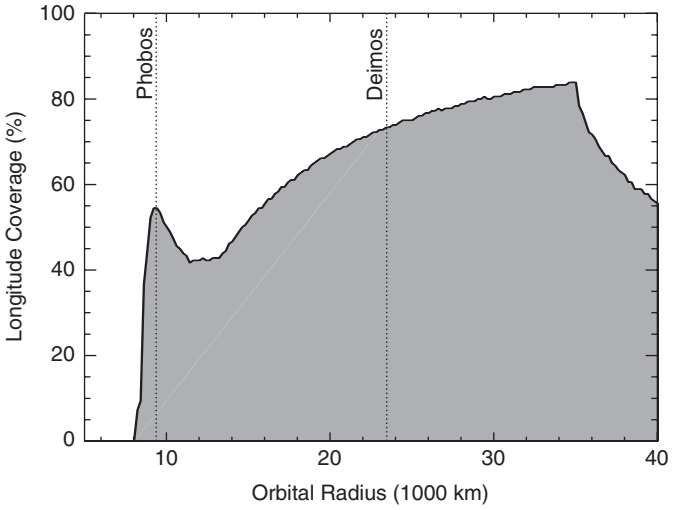

Fig. 9. Completeness of orbital coverage in our search for undiscovered moons. For a given orbital radius, the plot shows the fraction of initial longitudes that were covered in the search. A particular longitude is considered covered if a moon starting at that location would have been detected in at least three images.

images, motion smear could be as large as 28 pixels in 400 s. However, these images have still been useful because (a) they have finer overall sensitivity, and (b) a moon imaged near its maximum elongation would smear by a considerably smaller distance.

The completeness of our search, at the level of 50–80%, indicates that one or a few moons could easily have escaped our notice. However, it is clear that the Martian system cannot contain large numbers of tiny, unseen moons in the ~100 m size range. Perhaps perturbations by Phobos and Deimos render other orbital locations in the system dynamically unstable; alternatively, Phobos and Deimos may simply be the only two objects captured into Martian orbit in the Solar System's recent history. See Dones et al. (2006) for related dynamical discussions regarding the population of small Saturnian moons.

A recent survey for distant Martian satellites (Sheppard et al., 2004) nicely complements our search for closer moons. Both surveys are sensitive to moons with radii ~100 m, and both results are negative.

5. Discussion

A detection of the Phobos or Deimos rings would have been a great predictive success for ring science. In spite of the great diversity of planetary systems, a number of recurring themes have emerged. Dusty rings are associated with one or more small moons orbiting each of the gas giants. Thus, a thorough search for the putative Martian rings serves as a worthwhile test of our understanding of how dusty ring systems form. Because our conclusions about the Deimos ring are more tentative, we focus primarily on the Phobos ring in the discussion to follow.

The limits on τ of the Phobos and Deimos rings, 3×10^{-8} and 10^{-7}, respectively, rule out the upper predictions from papers summarized by Krivov and Hamilton (1997). In particular, the self-sustained Phobos ring model, with a predicted optical depth of $10^{-7\pm1}$, is most strongly constrained. Because the largest uncertainty is in the flux of interplanetary impactors, the self-sustained scenario has tighter error bars than the interplanetary impactor scenario. Our new upper limit appears to nearly rule out a self-sustained Phobos ring.

Accordingly, we revisit the dynamics of the Phobos ring to determine how firm this conclusion actually is. In particular, the combination of radiation pressure and Mars' oblateness drives particles smaller than about 30 μm to collide with Mars within a few years (Krivov et al., 1996; Hamilton, 1996; Ishimoto, 1996). This time scale is brief compared to the typical re-accretion time onto Phobos of about 30 years, so only larger particles are likely to form a self-sustaining population. But how secure is this lower limit?

None of the most sophisticated studies (Juhasz and Horanyi, 1995; Krivov et al., 1996; Ishimoto, 1996; Hamilton, 1996) carefully considered the effects of Mars' eccentricity over long time scales. Accordingly, we have undertaken new simulations of the Phobos dust ring including Mars' eccentricity, launching dust grains when Mars was at different points along its orbit. We also shut off radiation pressure in the planetary shadow, an effect not included in most previous studies. We find that the effects of shadowing are relatively unimportant while those of Mars' eccentricity are significant, in agreement with the discussion in Hamilton (1996).

Mars' eccentricity causes the strength of radiation pressure to vary periodically as the planet moves closer and further from the Sun. Using the nominal parameters from the earlier study (Hamilton, 1996), our new simulations show that this effect raises the minimum radius $r_{\min}$ of a dust grain that can avoid collision with Mars from 30 to 60 μm. Tinier grains are typically lost in time scales of 10–20 years. Furthermore, some grains up to 80 μm in radius are lost to the planet within 100 years. These additional losses leave fewer particles able to strike Phobos and eject additional material, thereby raising the possible self-sustaining population to larger sizes and lowering the overall predicted optical depth of the Phobos ring.

An additional complication is the uncertain mass density and light scattering properties of the ring particles. If these are other than the nominal values chosen in our modeling, the maximum particle size in the ring can increase or decrease significantly. If radiation is twice as strong as we have assumed, for example, then particles as large as 150 μm in radius could collide Mars.

We can estimate the implications of these changes in $r_{\min}$ by assuming the particles obey a power law size distribution of the form r^{-p}, where r is particle radius. In a power law, the total cross-section of particles varies as $r_{\min}^{3-p}$. A typical value for the slope $p \sim 3.5$, so increasing $r_{\min}$ by a

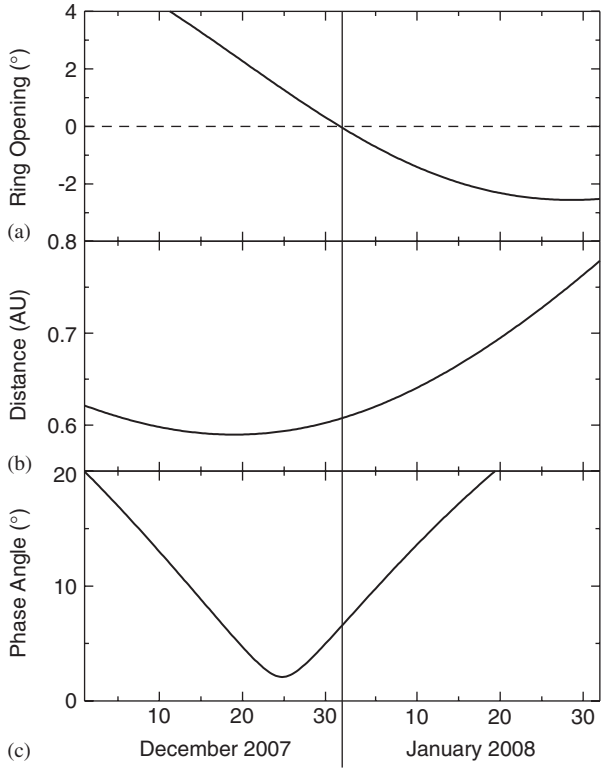

Fig. 10. The viewing geometry during an upcoming ring plane crossing in late 2007. The panels show the ring opening angle (a), the distance to Mars (b) and the phase angle (c), as a function of date during December 2007 and January 2008. The ring plane crossing occurs on December 31, at a range of 0.61 AU. For comparison, Mars' minimum distance to Earth is 0.59 AU on December 19 and opposition (minimum phase angle) is on December 25.

factor of two will reduce τ by a factor of $\sqrt{2}$. As a worst case, if r_{min} is increased from 30 to 150 μm and p is as large as 4, then τ is reduced by a factor of 5. These changes would place the Phobos ring below, but not far below, our detection threshold.

While our results are therefore not able to rule out a self-sustaining Phobos ring definitively, they are pushing the limits of what the models allow. We conclude that our results are more consistent with a ring in which interplanetary impactors dominate the production of new material. An order-of-magnitude improvement in our upper limit is probably necessary to fully rule out the self-sustaining scenario for the Phobos ring.

6. A future observing opportunity

We noted above the uniqueness of the May 2001 RPX. However, an opportunity that is almost as good occurs on December 31, 2007, when a Martian RPX occurs at a range to Earth of 0.61 AU (Fig. 10). This is only 20% further away than the May 2001 event. Meanwhile, the capabilities of our telescopes and instruments have increased substantially since 2001. For example, as noted above, the ACS instrument on HST is considerably more sensitive than the WFPC2. Moreover, Earth-based adaptive optics can now frequently rival HST in resolution and light-gathering capabilities.

December 2007 will therefore be an excellent opportunity to search once again for the Martian rings, with the potential to improve upon the limits placed in this paper. The viewing will be particularly ideal for the Deimos ring, which Krivov and Feofilov (2006) argue may have only barely escaped detection in 2001. Because this outer ring is so broad and diffuse, the slightly greater distance to Mars may turn out to be advantageous, because it will allow the Deimos ring to fit more easily into any instrument's field of view. Furthermore, this ring is so thick vertically that it is effectively edge-on to Earth whenever the ring opening angle is <2–3°. According to Fig. 10, that expands the optimal observing period to a duration of several weeks, making the observations less prone to obstacles that can arise around HST scheduling and Earth-based seeing. Krivov and Feofilov (2006) discuss this observing opportunity in greater detail.

Acknowledgments

Support for Hubble observing program GO-8579 was provided by NASA through a grant from the Space Telescope Science Institute, which is operated by the Association of Universities for Research in Astronomy, Inc., under NASA contract NAS5-26555. Additional support for MRS was provided by NASA's Planetary Geology and Geophysics Program. We thank Alexander Krivov and Hermann Boehnhardt for their helpful reviews of this manuscript.

References

Baggett, S., McMaster, M., Biretta, J., Burrows, C., Casertano, S., Fruchter, A., Ferguson, H., Gilliland, R., Gonzaga, S., Heyer, I., Holtzman, J., Koekemoer, A., Krist, J., Lubin, L., Mack, J., O'Dea, C., Kozhurina-Platais, V., Riess, A., Schultz, A., Stiavelli, M., Whitmore, B., Wiggs, M., 2002. HST WFPC2 Data Handbook, v. 4.0.

Burns, J.A., Showalter, M.R., Hamilton, D.P., Nicholson, P.D., de Pater, I., Ockert-Bell, M., Thomas, P., 1999. The formation of Jupiter's faint rings. Science 284 (5417), 1146–1150.

Dones, L., Showalter, M.R., Durisen, R.H., Honeycutt, R.K., Jurcevic, J.S., Tripoli, R., Strom, C., 2006. A search for Saturnian moonlets using the WIYN Telescope. Icarus, in press.

Dubinin, E.M., Lundin, R., Pissarenko, N.F., Barabash, S.V., Zakharov, A.V., Koskinen, H., Schwingenshuh, K., Yeroshenko, Y.G., 1990. Indirect evidences for a gas/dust torus along the Phobos orbit. Geophys. Res. Lett. 17, 861–864.

Duxbury, T.C., Ocampo, A.C., 1988. Mars: satellite and ring search from Viking. Icarus 76, 160–162.

Feibelman, W.A., 1967. Concerning the "D" ring of Saturn. Nature 214, 793–794.

Hamilton, D.P., 1996. The asymmetric time-variable rings of Mars. Icarus 119, 153–172.

Hamilton, D.P., Burns, J.A., 1994. Origin of Saturn's E ring: self-sustained, naturally. Science 264, 550–553.

Ishimoto, H., 1996. Formation of Phobos/Deimos dust rings. Icarus 122, 153–165.

Juhasz, A., Horanyi, M., 1995. Dust torus around Mars. J. Geophys. Res. 100 (E2), 3277–3284.

Krivov, A.V., Feofilov, A.G., 2006. Search for the putative dust belts of Mars: a 2007 opportunity. Planet. Space Sci., this issue.

Krivov, A.V., Hamilton, D.P., 1997. Martian dust belts: waiting for discovery. Icarus 128, 335–353.

Krivov, A.V., Sokolov, L.L., Dikarev, V.V., 1996. Dynamics of Mars-orbiting dust: effects of light pressure and planetary oblateness. Celest. Mech. Dyn. Astron. 63, 313–339.

Makuch, M., Krivov, A.V., Spahn, F., 2005. Long-term dynamical evolution of dusty ejecta from Deimos. Planet. Space Sci. 53, 357–369.

Nicholson, P.D., Showalter, M.R., Dones, L., French, R.G., Larson, S.M., Lissauer, J.J., McGhee, C.A., Seitzer, P., Sicardy, B., Danielson, G.E., 1996. Observations of Saturn's ring plane crossings in August and November 1995. Science 272, 509–515.

Sheppard, S.S., Jewitt, D., Kleyna, J., 2004. A survey for outer satellites of Mars: limits to completeness. Astron. J. 128 (5), 2542–2546.

Showalter, M.R., Lissauer, J.J., 2006. The second ring-moon system of Uranus: discovery and dynamics. Science 317, 973–977.

Showalter, M.R., Burns, J.A., de Pater, I., Hamilton, D.P., Horanyi, M., 2003. Recent Hubble observations of Jupiter's ring system. Bull. Am. Astron. Soc. 35 (#11.08).

Showalter, M.R., Burns, J.A., de Pater, I., Hamilton, D. P., Horanyi, M., 2005a. Jupiter's ring system: new results from Galileo, Voyager, Hubble and the Keck Telescope. Presentation at the ISSI Workshop on the Physics of Dusty Rings, Bern, Switzerland, June 20–24.

Showalter, M.R., Lissauer, J.J., de Pater, I., 2005b. The rings of Neptune and Uranus in the hubble space telescope. Bull. Am. Astron. Soc. 37 (#66.09).

Showalter, M.R., de Pater, I., Verbanac, G., Hamilton, D.P., Burns, J.A., 2006. Properties and dynamics of Jupiter's gossamer rings from Galileo, Voyager, Hubble and Keck images. Icarus, in press.

Smith, B.A., Soderblom, L.A., Johnson, T.V., Ingersoll, A.P., Collins, S.A., Shoemaker, E.M., Hunt, G.E., Masursky, H., Carr, M.H., Davies, M.E., Cook II, A.F., Boyce, J., Danielson, G.E., Owen, T., Sagan, C., Beebe, R.F., Veverka, J., Strom, R.G., McCauley, J.F., Morrison, D., Briggs, G.A., Suomi, V.E., 1979. The Jupiter system through the eyes of Voyager 1. Science 204, 951–972.

Soter, S., 1971. The dust belts of Mars. Cornell Center for Radiophysics and Space Research Report 462.